Supporting Information for "Theoretical Limits to the Anode Potential in Aqueous Mg-Air Batteries"

Leanne D. Chen,[†] *Jens K. Nørskov,*[†] *Alan C. Luntz**[†]

[†]SUNCAT Center for Interface Science and Catalysis, Department of Chemical Engineering, 443 Via Ortega, Stanford, California 94305-5025, United States and SLAC National Accelerator Laboratory, 2575 Sand Hill Road, Menlo Park, California 94025, United States

Convergence

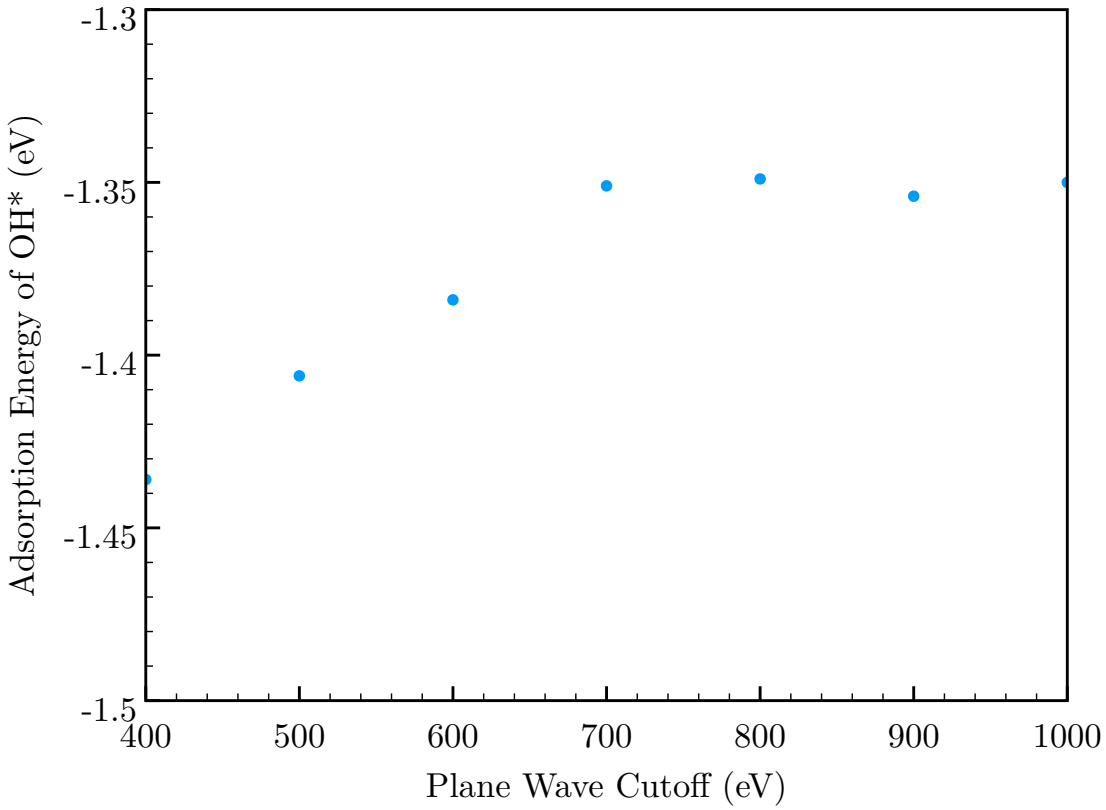

Figure S1. Convergence testing of hydroxide adsorption as a function of the plane wave cutoff (in all cases, density cutoff = plane wave cutoff × 10).

Plane wave and density cutoffs of 700 eV and 700 eV (respectively) were used, as they showed the first signs of convergence as seen in Figure S1.

Cl^- Adsorption

Analogous to hydroxide adsorption, we can represent chloride adsorption with the following equation

$$Mg + Cl^-_{(aq)} \rightleftharpoons MgCl^* + e^- \quad [1]$$

Where Mg represents a surface site, and MgCl* is the adsorbed state.

Table S1. Hydroxide and chloride adsorption energy comparisons for different sites, relative to the least stable site for each adsorbate (bridge for hydroxide, and atop for chloride).

Hydroxide	**Δ*E* (eV)**	**Chloride**	**Δ*E* (eV)**
Atop	Unstable	Atop	0
Bridge	0	Bridge	−0.39
FCC	−0.22	FCC	−0.47
HCP	−0.26	HCP	−0.47

We chose the HCP site for hydroxide as it was the most stable. For chloride, we note that the FCC and HCP sites are indistinguishable in terms of adsorption energy. We chose to conduct chloride adsorption studies at the HCP site for consistency.

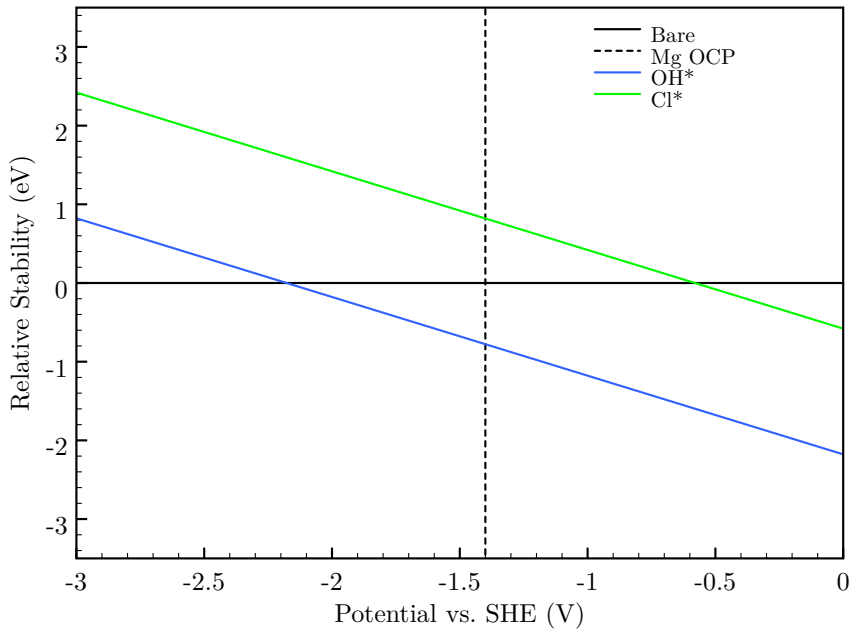

Figure S2. Surface stability diagram for adsorbed Cl* and OH* at pH 10.4 as a function of potential vs. the standard hydrogen electrode (SHE). The green line corresponds to chloride adsorption, and the blue line corresponds to hydroxide adsorption. The solid black line represents the bare Mg (0001) surface, and the vertical dashed black line represents the experimentally measured open-circuit potential of Mg vs. SHE as a reference.

It can be seen in Figure S2 that hydroxide adsorption is favored by ~1.5 eV compared to chloride adsorption across all potential ranges. The two lines are parallel due to an electron being released on the right-hand side in both cases, where the free energy change rises with decreasing applied potential. Therefore we only consider the role of hydroxide in the anodic dissolution of the Mg-air battery.

Water Stabilization

On Pt and other transition metals, it is known that a water bilayer stabilizes OH* on the surface,[1-3] thus it is critical to understand whether this stabilization plays a role in the case of Mg. Many different geometries of an adsorbed water bilayer structure were tested on the Mg (0001) bare surface. In all cases, it was observed that the hexagonal ice-like structure known to exist on Pt (from both theory and experiment)[4] is unstable on Mg. Instead, a distorted trefoil structure forms. This is because the metal-metal distance in a close-packed plane is much larger for Mg (3.21 Å) than it is for Pt (2.77 Å), where that in the latter happens to align quite well with the lattice constant of water ice.

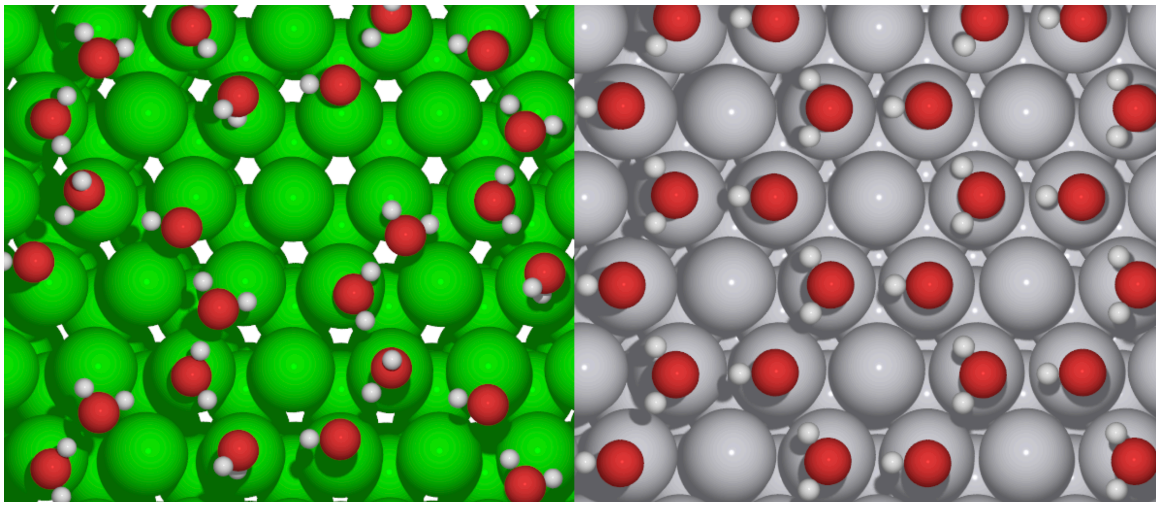

Figure S3. Pure water bilayer structures on Mg (left) and Pt (right). Green spheres represent Mg atoms, grey spheres represent Pt atoms, red spheres represent O atoms, and white spheres represent H atoms. Pt exhibits an archetypal hexagonal lattice, whereas Mg adopts a trefoil structure distorted from the former. This unusual behavior on Mg is caused by a much longer metal-metal distance in the close-packed plane, which does not agree with the water ice lattice constant.

The effect of water stabilization on adsorbed hydroxide was investigated by comparing the stability of the distorted water structure on Mg (shown in Figure S3) to a similar structure with one fewer proton. This represents the following process

$$Mg(H_2O)_8^* + OH^-_{(aq)} \rightleftharpoons Mg(H_2O)_7{}^*OH^* + H_2O^* + e^- \quad [1]$$

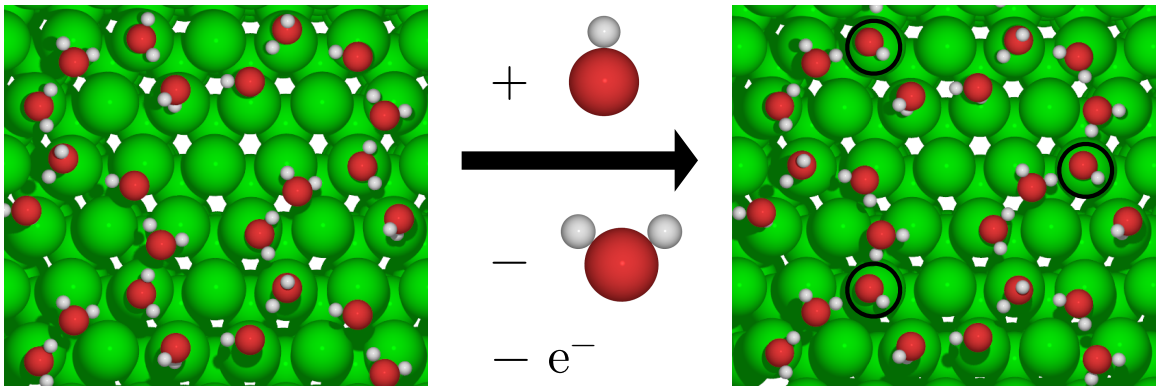

Figure S4. Schematic of OH^- adsorption to a magnesium surface in the presence of a water bilayer where OH* displaces one H_2O. The view here encompasses roughly three unit cells, therefore the OH* species in [1] (circled in black) appear three times.

and is schematically depicted in Figure S4. The subscript 8 after H_2O represents the number of water molecules in each unit cell, which implies eight different geometries for the structure $Mg(H_2O)_7{}^*OH^*$, as a proton can be taken off of any of the eight water molecules. Another possibility was tested where one extra OH* was placed roughly in the symmetry center of the trefoil, and represents instead

$$Mg(H_2O)_8^* + OH^-_{(aq)} \rightleftharpoons Mg(H_2O)_8{}^*OH^* + e^- \quad [2]$$

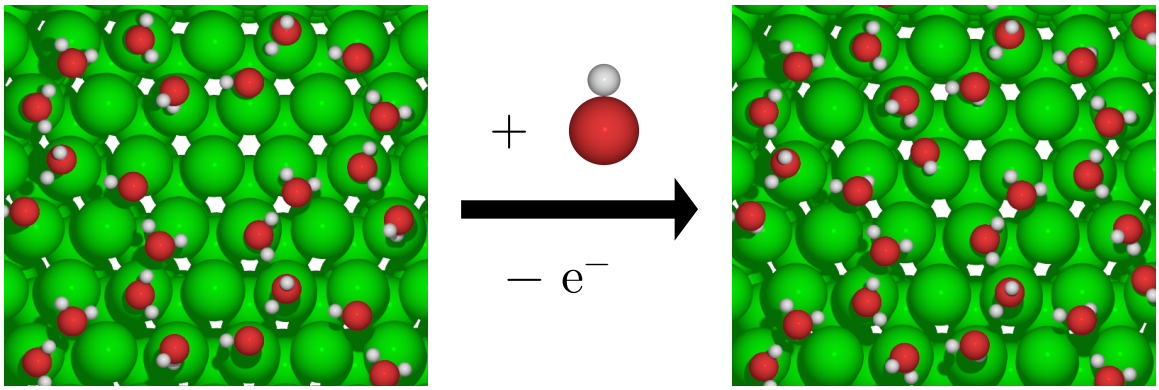

Figure S5. Schematic of OH^- adsorption to a magnesium surface in the presence of a water bilayer. Here, no water molecules are displaced, and the site of adsorption is roughly at the symmetry center of the trefoil.

This process is shown in Figure S5. We compare the free energy change of both types of processes to OH^- adsorption without a water bilayer, which is explained in the main text and repeated here for continuity

$$Mg + OH^-_{(aq)} \rightleftharpoons MgOH^* + e^- \quad [3]$$

Compared to the ΔG of OH^- adsorption without a surrounding water bilayer (described by [3]), the ΔGs of [1] and [2] were found to be less stable in all cases for many different geometries of both the pure H_2O bilayer, $Mg(H_2O)_8$*, and the H_2O/OH mixed bilayer, $Mg(H_2O)_7$*OH*. This is contrary to observations on the Pt surface, where the presence of the water bilayer stabilizes an OH* adsorbate by −0.3 eV on average.[1-3] We rationalize this by the lack of adequate hydrogen bonding to the adsorbate due to the much larger intermetallic distance in Mg. Moreover, water adsorption was also tested on the fully hydroxylated Mg (0001) surface at different H_2O concentrations. These structures show very little interaction between OH* and H_2O, which suggests that the OH*-covered surface is also hydrophobic.

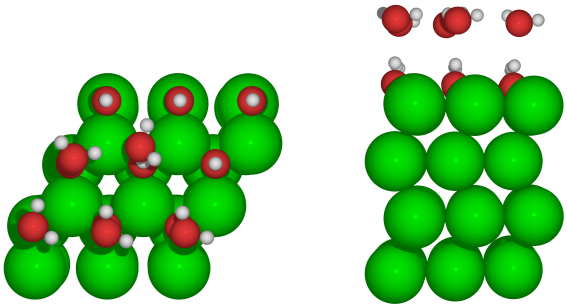

Figure S6. Water structure at a coverage of $^5/_9$. Left: top view. Right: side view.

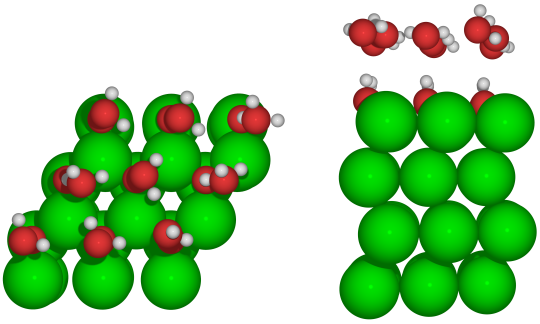

Figure S7. Water structure at a coverage of 1. Left: top view. Right: side view.

As Figure S6 and Figure S7 illustrate, both intra-adsorbate (H_2O-H_2O) and inter-adsorbate (H_2O-OH) interactions are small. Since the free energy of bulk liquid water is significantly lowered by extensive hydrogen bonding, it would be thermodynamically unfavorable to break these hydrogen bonds and form a structure with almost no hydrogen bonding both between the water molecules (due to the large lattice spacing of Mg) and between water and surface OH*. These observations suggest that water wets neither the bare Mg (0001) surface nor the OH*-covered Mg (0001) surface, therefore we do not include the effects of water on the adsorption energy of OH^-.

Construction of the Stepped and Kinked Surfaces

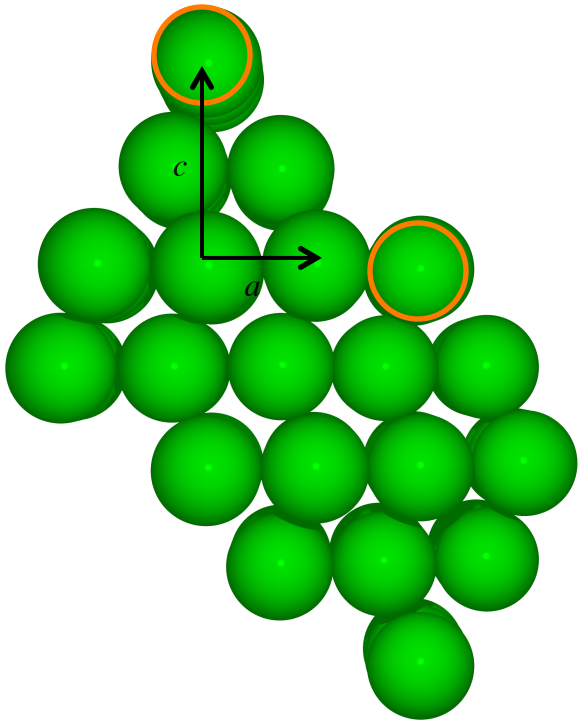

Figure S8. Stepped Mg surface. The cell is repeated once in the *a* direction and the two equivalent atoms are circled in orange. The close-packed planes are aligned horizontally to aid the eye.

The stepped surface was constructed by displacing one row of close-packed atoms in the (0001) facet by two lattice parameters in the *a* direction, and one lattice parameter in the *c* direction, as shown in Figure S8.

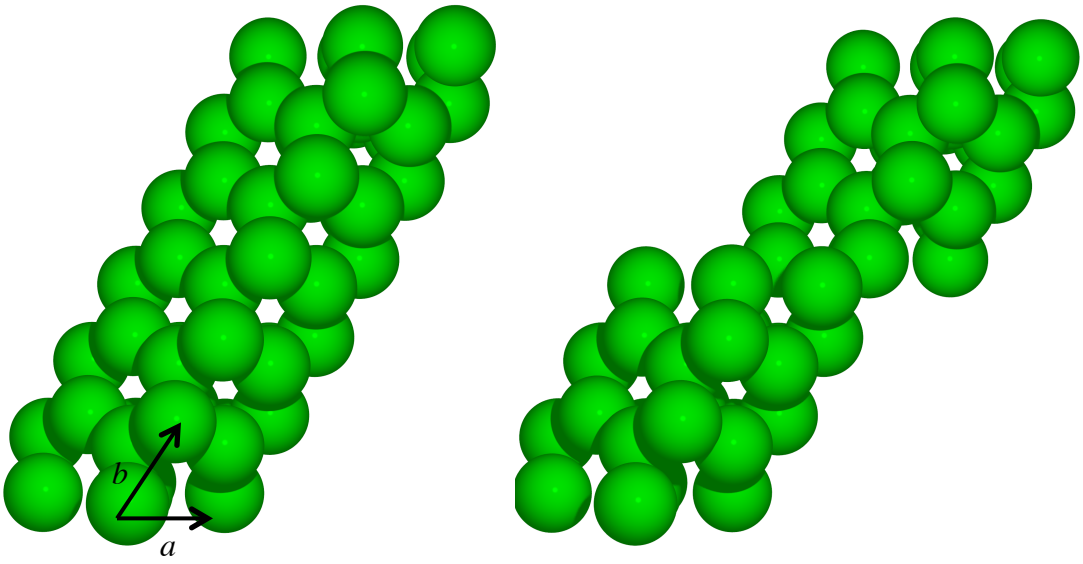

Figure S9. Comparison between the stepped (left) and kinked (right) Mg surfaces. The cells are repeated once in the *b* direction.

The kinked surface was obtained by displacing the *b* lattice vector one lattice parameter in the *a* direction in the stepped surface, as can be seen by the offset of exactly one atom in the *a* direction in adjacent unit cells on the right side of Figure S9.

Calculation Details

Electronic structure calculation parameters for these calculations are summarized in the main text; the only differences are outlined in the following. The pure H_2O and H_2O/OH bilayer structures were calculated with the RPBE exchange-correlation functional as van der Waals contributions to the water structure are anticipated to not be dominant. The plane wave and density cutoffs were 400 eV and 4000 eV, respectively. These structures were calculated in a $(2\sqrt{3}\times2\sqrt{3})R60°$ cell, where the vacuum separation was at least 16 Å between the slabs in all cases.

(1) Nørskov, J. K.; Rossmeisl, J.; Logadottir, A.; Lindqvist, L.; Kitchin, J. R.; Bligaard, T.; Jónsson, H. Origin of the Overpotential for Oxygen Reduction at a Fuel-Cell Cathode. *J. Phys. Chem. B* **2004**, *108*, 17886–17892.

(2) Rossmeisl, J.; Logadottir, A.; Nørskov, J. K. Electrolysis of Water on (Oxidized) Metal Surfaces. *Chemical Physics* **2005**, *319*, 178–184.

(3) Rossmeisl, J.; Nørskov, J. K.; Taylor, C. D.; Janik, M. J.; Neurock, M. Calculated Phase Diagrams for the Electrochemical Oxidation and Reduction of Water Over Pt(111). *J. Phys. Chem. B* **2006**, *110*, 21833–21839.

(4) Ogasawara, H.; Brena, B.; Nordlund, D.; Nyberg, M.; Pelmenschikov, A.; Pettersson, L. G. M.; Nilsson, A. Structure and Bonding of Water on Pt(111). *Phys. Rev. Lett.* **2002**, *89*, 276102.